Numerical assessment of pressure, velocity, and stress post-processing strategies for the Biot's problem

Giovanni Taraschi[1], Maicon R. Correa[1]

[1]*Departamento de Matemática Aplicada, IMECC, Unicamp*
Rua Sérgio Buarque de Holanda, 651, 13083-859, Campinas/SP, Brasil
gitaraschi@gmail.com, maicon@ime.unicamp.br

Abstract. In the context of the displacement-pressure formulation for the Biot's problem, the present work explores some possibilities of Finite Element post-processings to improve the accuracy of the pressure field, the Darcy velocity, and the effective stress. Numerical experiments illustrate the performance of the different strategies and compare their results with the native approximations obtained through the use of the lowest-order Taylor-Hood space in the displacement-pressure Galerkin method. Our results indicate that the post-processing strategies presented significantly improve the approximation of the velocity and effective stress fields. The pressure field, on the other hand, does not benefit as much from the strategies considered here.

Keywords: Finite Element Method, Biot's problem, Post-processing strategies

1 The two-dimensional Biot's problem

Poroelasticity problems describe the coupling between the mechanics of an elastic porous matrix saturated with a Newtonian fluid and the flow of such fluid through the voids of the porous matrix. The study of such systems dates back to the pioneering work of Terzaghi [1], where a one-dimensional model for soil consolidation was developed. The work of Terzaghi was later generalized to incorporate the compression of fluid and soil particles by Biot [2], leading to what is now the mathematical foundations of poroelasticity problems. Applications of Biot's model in poroelasticity range from consolidation problems in reservoir engineering, such as oil extraction [3] and water resources management [4], to biomedical simulations of living tissues [5, 6].

Let $\Omega \subset \mathbb{R}^2$ be an open and bounded polygonal domain occupied by an elastic porous matrix saturated with a Newtonian fluid. The two-dimensional Biot's model is mathematically described by the following set of equations, which need to be satisfied for every time instant t in the time domain $T = (t_i, t_f]$ and every point $\boldsymbol{x} \in \Omega$

$$\boldsymbol{\sigma} = \boldsymbol{C}\boldsymbol{\varepsilon}(\boldsymbol{u}), \tag{1a}$$

$$\boldsymbol{z} = -\boldsymbol{\mathcal{K}}\nabla p, \tag{1b}$$

$$-\operatorname{div}\boldsymbol{\sigma} + \alpha\nabla p = \boldsymbol{f}, \tag{1c}$$

$$\alpha \operatorname{div}\boldsymbol{u}_t + \operatorname{div}\boldsymbol{z} = g. \tag{1d}$$

Equation (1a) is the Hooke's law, which relates the second-order effective stress tensor $\boldsymbol{\sigma} : \Omega \times T \to \mathbb{S} = \mathbb{R}^{\text{sym}}_{2\times 2}$ with the displacement vector field $\boldsymbol{u} : \Omega \times T \to \mathbb{R}^2$. Here, $\boldsymbol{\varepsilon}(\boldsymbol{u}) = \left(\nabla\boldsymbol{u} + \nabla^T\boldsymbol{u}\right)/2$ denotes the symmetric part of the gradient of $\boldsymbol{u}$, and $\boldsymbol{C}$ is a bounded, symmetric, and uniformly positive definite fourth-order tensor called the Elasticity tensor. When the porous matrix is made of a homogeneous and isotropic material, the elasticity tensor is defined by the Lamé constants μ and λ according to

$$\boldsymbol{C}\boldsymbol{S} = 2\mu\boldsymbol{S} + \lambda \operatorname{tr}\boldsymbol{S}, \quad \forall \boldsymbol{S} \in \mathbb{M} = \mathbb{R}_{2\times 2}. \tag{2}$$

The relation between the pore pressure $p : \Omega \times T \to \mathbb{R}$ and the percolation velocity $\boldsymbol{z} : \Omega \times T \to \mathbb{R}^2$ of the fluid relative to the porous matrix is described by the Darcy's law (1b). In this equation, $\boldsymbol{\mathcal{K}}$ is a bounded, symmetric, and uniformly positive definite second-order tensor defined as the quotient between the porous matrix permeability and the fluid viscosity.

The conservation of the linear momentum is stated by the equilibrium equation (1c), where $\boldsymbol{f} : \Omega \times T \to \mathbb{R}^2$ is a prescribed function describing the distributed load over the elastic body and the div operator acts row-wise over $\boldsymbol{\sigma}$. Finally, eq. (1d) is referred to as the continuity equation and models the mass conservation property, with $g : \Omega \times T \to \mathbb{R}$ being a given source/sink function and the sub-index t in $\operatorname{div} \boldsymbol{u}_t$ denoting the partial derivative with respect to the time variable. In both eq. (1c) and (1d), α is the Biot–Willis constant, which is positive and usually close to one.

By substituting (1a) in (1c) and (1b) in (1d), we can obtain a partial differential system written only in terms of the displacement field and the pore pressure

$$-\operatorname{div}(\boldsymbol{C}\boldsymbol{\varepsilon}(\boldsymbol{u})) + \alpha \nabla p = \boldsymbol{f} \quad \text{in } \Omega, \tag{3a}$$

$$\alpha \operatorname{div} \boldsymbol{u}_t - \operatorname{div}(\boldsymbol{\mathcal{K}} \nabla p) = g \quad \text{in } \Omega. \tag{3b}$$

To obtain a well posed differential problem, system (3) must be accompanied by boundary and initial conditions. For simplicity of presentation, we shall only consider Dirichlet boundary conditions in this work, meaning that the values of $\boldsymbol{u}$ and p are prescribed in the boundary $\Gamma = \partial\Omega$

$$\boldsymbol{u} = \boldsymbol{u}_D \;\text{ and }\; p = p_D \quad \text{ on } \Gamma. \tag{4}$$

We remark that the results presented here are still valid if Neumann conditions were employed as well. As for the initial condition, we simply assume that the functions $\boldsymbol{u}(\boldsymbol{x}, t_i)$ and $p(\boldsymbol{x}, t_i)$ are prescribed. In some applications, however, such initial conditions have to be computed through an auxiliary problem. For instance, in Murad and Loula [7, 8] and Murad et al. [9], the initial conditions are obtained by the solution of a Stokes-like problem.

2 A Finite Element solution for the Biot's problem

The Finite Element Method for the approximation of Biot's problem (3) discussed in this work is based on the displacement-pressure variational formulation. In that formulation, the sought solution $(\boldsymbol{u}, p) \in H^1(\Omega, \mathbb{R}^2) \times H^1(\Omega)$ must satisfy the Dirichlet boundary conditions (4) and the following system of integral equations

$$\int_\Omega \boldsymbol{C}\boldsymbol{\varepsilon}(\boldsymbol{u}) : \boldsymbol{\varepsilon}(\boldsymbol{v}) \,\mathrm{d}x + \int_\Omega \alpha \nabla p \cdot \boldsymbol{v} \,\mathrm{d}x = \int_\Omega \boldsymbol{f} \cdot \boldsymbol{v} \,\mathrm{d}x \qquad \forall \boldsymbol{v} \in H^1_0(\Omega, \mathbb{R}^2), \tag{5a}$$

$$\int_\Omega \alpha \operatorname{div} \boldsymbol{u}_t \, q \,\mathrm{d}x + \int_\Omega (\boldsymbol{\mathcal{K}} \nabla p) \cdot \nabla q \,\mathrm{d}x = \int_\Omega g \, q \,\mathrm{d}x \qquad \forall q \in H^1_0(\Omega), \tag{5b}$$

where $H^1(\Omega)$ is the classical Sobolev space over Ω, $H^1(\Omega, \mathbb{R}^2) = H^1(\Omega) \times H^1(\Omega)$, and $H^1_0(\Omega) \subset H^1(\Omega)$ and $H^1_0(\Omega, \mathbb{R}^2) \subset H^1(\Omega, \mathbb{R}^2)$ are the subspaces with vanishing trace on Γ.

To obtain a fully discrete system based on formulation (5), a discretization scheme for the time derivative needs to be set. To do so, we first divide the time domain T into $M + 1$ points $t_m = t_i + m\Delta t$, with m ranging from 0 to M and $\Delta t = (t_f - t_i)/M$ denoting the time step. Here, we chose the backward Euler method for the time discretization, which leads to the following approximation

$$\operatorname{div} \boldsymbol{u}_t(\boldsymbol{x}, t_m) \approx \frac{\operatorname{div} \boldsymbol{u}(\boldsymbol{x}, t_m) - \operatorname{div} \boldsymbol{u}(\boldsymbol{x}, t_{m-1})}{\Delta t}, \tag{6}$$

for every $m = 1, \ldots, M$.

Next, a spatial discretization must be defined. In Finite Element Methods based on formulation (5), this is done by setting finite-dimensional subspaces $\mathcal{U}_h \subset H^1(\Omega, \mathbb{R}^2)$ and $\mathcal{P}_h \subset H^1(\Omega)$. We also need to consider their restrictions

$$\mathcal{U}_{h,0} = \{\boldsymbol{v} \in \mathcal{U}_h \,:\, \boldsymbol{v} = 0 \text{ on } \Gamma\} \subset H^1_0(\Omega, \mathbb{R}^2) \quad \text{and} \quad \mathcal{P}_{h,0} = \{q \in \mathcal{P}_h \,:\, q = 0 \text{ on } \Gamma\} \subset H^1_0(\Omega). \tag{7}$$

By combining the use of the finite-dimensional spaces $\mathcal{U}_h$ and $\mathcal{P}_h$ and their respective restrictions with the backward Euler approximation (6), we obtain the following fully-discrete problem: For each $m = 1, \ldots, M$, find the pair $(\boldsymbol{u}_h^m, p_h^m) \in \mathcal{U}_h \times \mathcal{P}_h$, satisfying the Dirichlet boundary conditions (4), such that

$$\int_\Omega \boldsymbol{C}\boldsymbol{\varepsilon}(\boldsymbol{u}_h^m) : \boldsymbol{\varepsilon}(\boldsymbol{v}) \,\mathrm{d}x + \int_\Omega \nabla p_h^m \cdot \boldsymbol{v} \,\mathrm{d}x = \int_\Omega \boldsymbol{f}(t_m) \cdot \boldsymbol{v} \,\mathrm{d}x \qquad \forall \boldsymbol{v} \in \mathcal{U}_{h,0}, \tag{8a}$$

$$\int_\Omega \alpha \operatorname{div} \boldsymbol{u}_h^m \, w \,\mathrm{d}x + \Delta t \int_\Omega (\boldsymbol{\mathcal{K}} \nabla p_h^m) \cdot \nabla w \,\mathrm{d}x = \Delta t \int_\Omega g(t_m) \, w \,\mathrm{d}x + \int_\Omega \alpha \operatorname{div} \boldsymbol{u}_h^{m-1} \, w \,\mathrm{d}x \quad \forall w \in \mathcal{P}_{h,0}, \tag{8b}$$

where $\boldsymbol{u}_h^m$ and p_h^m are the approximations for the displacement and pressure fields at $t = t_m$.

The spaces $\mathcal{U}_h$ and $\mathcal{P}_h$ chosen in this work were the lowest-order Taylor-Hood spaces [10, 11]. Let $\mathcal{T}_\mathrm{h}$ be a regular triangulation of the domain Ω, and denote by $P_r(K)$ the space of polynomials of total degree less than or equal to r over a triangular element $K \in \mathcal{T}_\mathrm{h}$. When the lowest-order Taylor-Hood space is applied to problem (8), the displacement approximation space $\mathcal{U}_h$ is given by

$$P_2(\mathcal{T}_\mathrm{h}, \mathbb{R}^2) = \{\boldsymbol{v} \in \mathcal{C}^0(\Omega, \mathbb{R}^2) \,:\, \boldsymbol{v}|_K \in P_2(K) \times P_2(K),\ \forall K \in \mathcal{T}_\mathrm{h}\}, \tag{9}$$

while the pressure approximation space $\mathcal{P}_h$ is set as

$$P_1(\mathcal{T}_\mathrm{h}) = \{q \in \mathcal{C}^0(\Omega) \,:\, q|_K \in P_1(K),\ \forall K \in \mathcal{T}_\mathrm{h}\}. \tag{10}$$

In eq. (9) and (10), $\mathcal{C}^0(\Omega)$ and $\mathcal{C}^0(\Omega, \mathbb{R}^2)$ denote the spaces of scalar and vector functions that are continuous over the domain Ω.

Existence and uniqueness of solution for problem (8) when using the lowest-order Taylor-Hood spaces are discussed, for instance, in Murad and Loula [8] and Murad et al. [9]. The fact that the Taylor-Hood spaces are inf-sup stable (see Chapter 8.8 of Boffi et al. [11]) helps to avoid the appearance of spurious pressure oscillations [8, 9]. Nevertheless, in the presence of strong pressure gradients, oscillations can appear even for inf-sup stable elements, as shown by Aguilar et al. [12].

2.1 Error estimates for the fully discrete problem

Assume that the exact solutions of problem (3) for the displacement and pressure fields are regular enough, and consider

$$\phi(t) = |\boldsymbol{u}(t)|_3 + |p(t)|_{2,\Omega} + |\boldsymbol{u}_t(t)|_3 + |\operatorname{div} \boldsymbol{u}_{tt}(t)|_2, \tag{11}$$

with $|\cdot|_r$ being the semi-norms in the scalar and vector H^r Sobolev spaces and the sub-index tt in $\operatorname{div} \boldsymbol{u}_{tt}$ denoting the second order time derivative.

Under these conditions, Murad and Loula [8] develops the convergence analysis for the discrete problem (8). In particular, the authors show that the approximated solutions $(\boldsymbol{u}_h^m, p_h^m)$ obtained through (8) using the lowest-order Taylor-Hood spaces satisfy

$$\|\boldsymbol{\varepsilon}(\boldsymbol{u}(t_m) - \boldsymbol{u}_h^m)\|_0 \leq C(h^2 + \Delta t) \sup_{t \in T} \phi(t) \quad \text{and} \quad \|\nabla(p(t_m) - p_h^m)\|_0 \leq C(h + \Delta t) \sup_{t \in T} \phi(t), \tag{12}$$

where $\|\cdot\|_0$ is the L^2 norm over Ω, h is the mesh parameter associated with the triangulation $\mathcal{T}_\mathrm{h}$, and C are constants independent of h and Δt. We draw attention to the fact that the convergence of ∇p_h^m is only linear in space, being one order lower than the convergence of $\boldsymbol{\varepsilon}(\boldsymbol{u}_h^m)$.

2.2 Approximations for the velocity and effective stress

In many applications, the percolation velocity $\boldsymbol{z}$, also known as the Darcy velocity, and the effective stress $\boldsymbol{\sigma}$ are variables of main interest [13]. However, methods based on the displacement-pressure system (3), such as (8), do not offer native approximations for such variables, which then need to be post-processed. The simplest way to obtain approximations for $\boldsymbol{z}$ and $\boldsymbol{\sigma}$ from the solutions $(\boldsymbol{u}_h^m, p_h^m)$ provided by (8) is by applying Hooke's (1a) and Darcy's (1b) laws element-wise

$$\boldsymbol{z}_{h,L}^m|_K = -\boldsymbol{\mathcal{K}} \nabla p_h^m|_K,\ \forall K \in \mathcal{T}_\mathrm{h}, \tag{13a}$$

$$\boldsymbol{\sigma}_{h,L}^m|_K = \boldsymbol{C}\boldsymbol{\varepsilon}(\boldsymbol{u}_h^m|_K),\ \ \forall K \in \mathcal{T}_\mathrm{h}\,. \tag{13b}$$

It is easy to verify from (12) that the local approximations defined by (13) satisfy the following error bounds

$$\|\boldsymbol{\sigma} - \boldsymbol{\sigma}_{h,L}^m\|_{0,\Omega} \leq C(h^2 + \Delta t) \sup_{t \in T} \phi(t) \quad \text{and} \quad \|\boldsymbol{z} - \boldsymbol{z}_{h,L}^m\|_{0,\Omega} \leq C(h + \Delta t) \sup_{t \in T} \phi(t), \tag{14}$$

where $\phi(t)$ is defined as in (11).

Approximations for the Darcy velocity are desired to belong to the $H(\operatorname{div}, \Omega, \mathbb{R}^2)$ space, meaning that the vector entries and its divergence are square integrable. If the Darcy velocity approximation belongs to $H(\operatorname{div}, \Omega, \mathbb{R}^2)$, its normal component is continuous across inter-element boundaries, which is important to guarantee good mass-conservation properties. Similarly, the effective stress approximation is desired to belong to $H(\operatorname{div}, \Omega, \mathbb{M})$, which is the space of 2×2 tensors such that each row belongs to $H(\operatorname{div}, \Omega, \mathbb{R}^2)$. For the effective stress, belonging to $H(\operatorname{div}, \Omega, \mathbb{M})$ is related to the balance of interior tractions. Unfortunately, strategies (13a) and (13b), although simple and with almost no extra computational cost added, lead to fully discontinuous approximations across inter-element boundaries, and therefore are not $H(\operatorname{div})$-conforming.

3 H(div)-conforming post-processing strategies

In this section, we propose more sophisticated post-processing strategies for the recovery of approximated velocity and stress fields from the original solution $(\boldsymbol{u}_h^m, p_h^m)$. Both strategies discussed here rely on the solution of a new global problem, rather than simple local computations. This change, although being more expensive from the computational perspective, brings benefits. Not only the post-processed solutions are $H(\mathrm{div})$-conforming, they also present better spatial convergence rates in some norms, as we shall verify in the numerical experiments of Section 4.

3.1 Global mixed post-processing for the pressure and Darcy velocity

In Murad and Loula [7, 8], the authors use an H^1-conforming variational form of the continuity equation (1d) to construct a post-processing strategy for the pressure field. That strategy is able to improve the spatial convergence in the approximation of p and ∇p, but proper approximations for the Darcy velocity are still lacking. In the present work, we use a mixed form of (1d) instead, in which the new variables are the post-processed pressure $p_{h,G}^m$ and the $H(\mathrm{div})$-conforming approximation for the Darcy velocity $\boldsymbol{z}_{h,G}^m$.

Denote by $L^2(\Omega)$ the space of square integrable scalar funcitons, and let $\mathcal{Z}_h \subset H(\mathrm{div}, \Omega, \mathbb{R}^2)$ and $\mathcal{P}_{h,G} \subset L^2(\Omega)$ be finite-dimensional subspaces. The mixed post-processing proposed here consists in finding $(z_{h,G}^m, p_{h,G}^m) \in \mathcal{Z}_h \times \mathcal{P}_{h,G}$ such that

$$\int_\Omega \boldsymbol{\mathcal{K}}^{-1}\, \boldsymbol{z}_{h,G}^m \cdot \boldsymbol{w}\,\mathrm{d}x - \int_\Omega p_{h,G}^m \,\mathrm{div}\,\boldsymbol{w}\,\mathrm{d}x = \int_\Gamma p_D(\boldsymbol{w}\cdot\boldsymbol{n})\,\mathrm{d}s \qquad \forall \boldsymbol{w} \in \mathcal{Z}_h, \tag{15a}$$

$$\int_\Omega \mathrm{div}\,\boldsymbol{z}_{h,G}^m\, q\,\mathrm{d}x = \int_\Omega g\, q\,\mathrm{d}x - \frac{1}{\Delta t}\int_\Omega \alpha\ \mathrm{div}(\boldsymbol{u}_h^m - \boldsymbol{u}_h^{m-1})\, q\,\mathrm{d}x \qquad \forall q \in \mathcal{P}_{h,G}, \tag{15b}$$

where p_D is the Dirichlet boundary condition established in (4), and $(z_{h,G}^m, p_{h,G}^m)$ approximate the velocity and pressure fields at $t = t_m$.

The adopted velocity approximation space is the Raviart-Thomas space $RT_1(\mathcal{T}_\mathrm{h}, \mathbb{R}^2)$ [14], whose construction for triangular meshes can be found in Chapter 2.3 of Boffi et al. [11]. To ensure the existence and uniqueness of solution for problem (15), the accompanying pressure approximation space needs to be set as

$$P_1^d(\mathcal{T}_\mathrm{h}) = \{q \in L^2(\Omega)\ :\ q|_K \in P_1(K),\ \forall K \in \mathcal{T}_\mathrm{h}\}. \tag{16}$$

Notice that in (16) we do not require continuity over Ω, allowing for pressure approximations that are discontinuous across inter-element boundaries.

Although we did not develop the convergence analysis for strategy (15), which will be the theme of future works, the numerical experiments of Section 4 show that, if the lowest-order Taylor-Hood space was used to obtain the original approximations $(\boldsymbol{u}_h^m, p_h^m)$, $\boldsymbol{z}_{h,G}^m$ has a spatial convergence one order higher than the local approximation $\boldsymbol{z}_{h,L}^m$ obtained by (13a).

3.2 Global post-processing for the effective stress

We now present a global $H(\mathrm{div})$-conforming post-processing strategy for the effective stress. Such a strategy is inspired by the post-processing technique proposed by Loula et al. [13], and recently applied to nearly-incompressible elasticity problems in Taraschi et al. [15]. The strategy presented here can be viewed as a generalization of the strategy originally proposed by Murad and Loula [7].

Let $\boldsymbol{u}_h^m$ be the approximated displacement field at $t = t_m$ computed through (8) and $\mathfrak{g}_h^m$ an approximation for $\nabla p(t_m)$. Given $\mathcal{S}_h$ a finite-dimensional subspace of $H(\mathrm{div}, \Omega, \mathbb{M})$, the stress recover technique consists in finding $\boldsymbol{\sigma}_{h,G}^m \in \mathcal{S}_h$ such that

$$\int_\Omega \boldsymbol{A}\boldsymbol{\sigma}_{h,G}^m : \boldsymbol{\tau}\,\mathrm{d}x + \int_\Omega \mathrm{div}\,\boldsymbol{\sigma}_{h,G}^m \cdot \mathrm{div}\,\boldsymbol{\tau}\,\mathrm{d}x = \int_\Omega \boldsymbol{\varepsilon}(\boldsymbol{u}_h^m) : \boldsymbol{\tau}\,\mathrm{d}x + \int_\Omega (\alpha\mathfrak{g}_h^m - \boldsymbol{f}(t_m))\cdot \mathrm{div}\,\boldsymbol{\tau}\,\mathrm{d}x, \quad \forall \boldsymbol{\tau} \in \mathcal{S}_h, \tag{17}$$

where $\boldsymbol{A}$ is the Compliance tensor, defined as the inverse of the elasticity tensor $\boldsymbol{C}$.

Notice that the first terms in the right and left-hand sides of (17) came from a weak version of the constitutive equation (1a). Meanwhile, the remaining terms of (17) are obtained by penalizing the residuals of the equilibrium equation (1c). For the purposes of this work, we shall set $\mathcal{S}_h$ as the Raviart-Thomas based tensor space $RT_1(\mathcal{T}_\mathrm{h}, \mathbb{M})$, defined as the space of tensors such that each row is a vector of $RT_1(\Omega, \mathbb{R}^2)$.

The most natural choice for $\mathfrak{g}_h^m$ is the gradient of the original pressure approximation. However, because ∇p_h^m converges only linearly in space, this option can deteriorate the overall performance of strategy (15). A better option, as we verified experimentally in Section 4, is setting $\mathfrak{g}_h^m = -\boldsymbol{\mathcal{K}}^{-1}\, \boldsymbol{z}_{h,G}^m$, for which optimal orders are obtained in the $H(\mathrm{div})$ norm.

4 Numerical experiments

The numerical experiments performed in this section have the goal of measuring the spatial convergence of the post-processing strategies discussed in Section 3. For that, we solve the model problem (3) setting $T = (0, 1]$, Ω as the unit square $(0, 1) \times (0, 1)$, and $\alpha = 1$. The second-order tensor $\boldsymbol{\mathcal{K}}$ was set as the identity tensor, while $\boldsymbol{C}$ is defined as in (2) taking $\mu = 1$ and $\lambda = 1.5$. Finally, the source terms $\boldsymbol{f}$ and g were chosen so the exact solutions for the displacement and pressure fields were given by

$$\boldsymbol{u}(\boldsymbol{x}, t) = \begin{bmatrix} t\sin(\pi x)\sin(\pi y) \\ t\sin(\pi x)\sin(\pi y) \end{bmatrix} \quad \text{and} \quad p(\boldsymbol{x}, t) = \frac{e^{t(x+y)}}{2}.$$

Notice that $\operatorname{div} \boldsymbol{u}$ is linear on t, meaning that the backward Euler method can exactly approximate the time derivative $\operatorname{div} \boldsymbol{u}_t$. This implies that the approximation errors are dominated by the error in the spatial approximation, enabling us to easily measure the spatial convergence of the proposed methods.

To solve that problem, the domain Ω was first divided into $n \times n$ squares. Each square was then subdivided into two triangles by the diagonal linking its southwest corner with the northeast one, resulting in meshes with $2n^2$ triangular elements. The values for n were set as powers of 2 ranging from 2 to 128. For the time discretization, Δt was kept fixed as 0.05. For each mesh, approximated solutions $(\boldsymbol{u}_h^m, p_h^m)$ were obtained by solving the system (8) with the lowest-order Taylor-Hood spaces.

Next, we compute the Darcy velocity approximations $\boldsymbol{z}_{h,L}^m$ and $\boldsymbol{z}_{h,G}^m$ using (13a) and (15) respectively. From the mixed method (15) we also obtain the post-processed pressure field $p_{h,G}^m$. For each value of n, we measure the pressure and velocity approximation errors in the L^2 norm at the final time $t_m = 1$. In Fig. 1, those results are plotted in $-\log_{10}(h) \times \log_{10}(\|error\|_0)$ graphs, from which we could numerically assess the spatial convergence order of each method. In that same figure, we also present results for the divergence of the Darcy velocity. A visual comparison between the first component of the Darcy velocity approximations $\boldsymbol{z}_{h,L}^m$ and $\boldsymbol{z}_{h,G}^m$ can be found in Fig. 3.

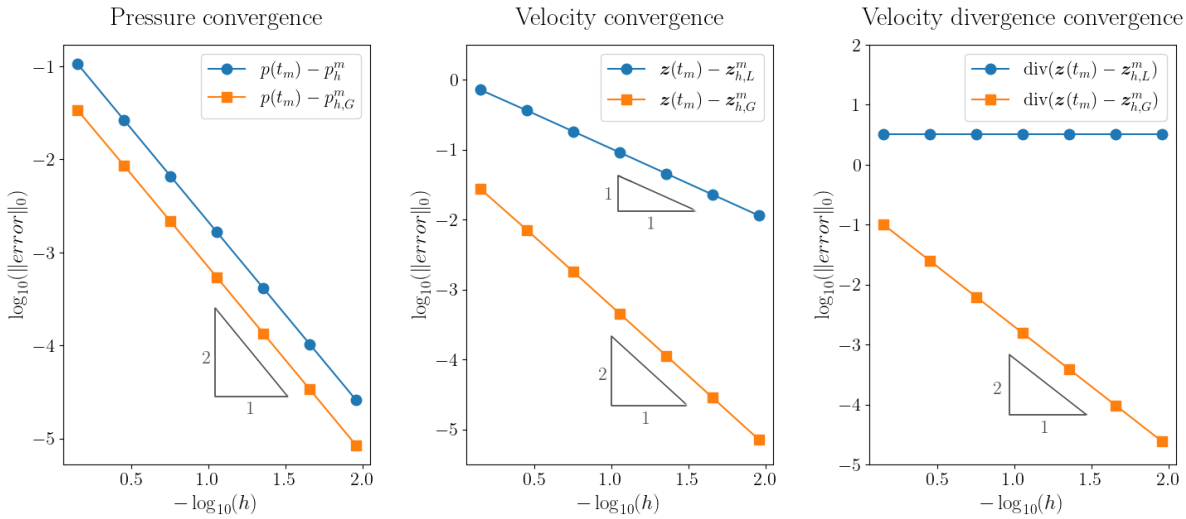

Figure 1. Convergence results for the approximation of the pressure (left), Darcy velocity (center), and divergence of the Darcy velocity (right). All the errors were measured at $t_m = 1$.

Finally, the approximations for the effective stress $\boldsymbol{\sigma}_{h,L}^m$ and $\boldsymbol{\sigma}_{h,G}^m$ are computed through (13) and (17). For the $H(\mathrm{div})$-conforming strategy (17), we set $\mathfrak{g}_h^m$ as both ∇p_h^m and $-\boldsymbol{\mathcal{K}}^{-1}\, \boldsymbol{z}_{h,G}^m$. Spatial convergence results for the stress approximation are presented through $-\log_{10}(h) \times \log_{10}(\|error\|_0)$ graphs in Fig. 2.

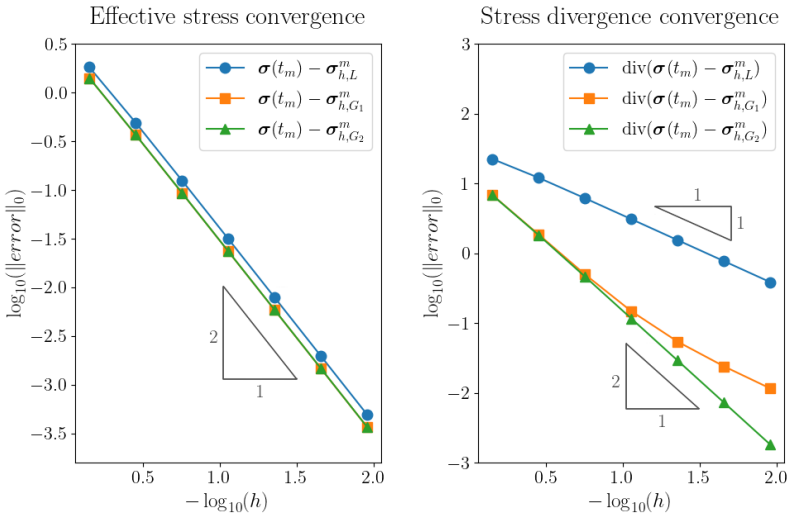

Figure 2. Convergence results for the approximation of the effective stress (left) and its divergence (right). The approximations $\boldsymbol{\sigma}^m_{h,G_1}$ and $\boldsymbol{\sigma}^m_{h,G_2}$ are obtained through (17) setting $\mathfrak{g}^m_h = \nabla p^m_h$ and $\mathfrak{g}^m_h = -\boldsymbol{\mathcal{K}}^{-1}\,\boldsymbol{z}^m_{h,G}$, respectively. All the errors were measured at $t_m = 1$.

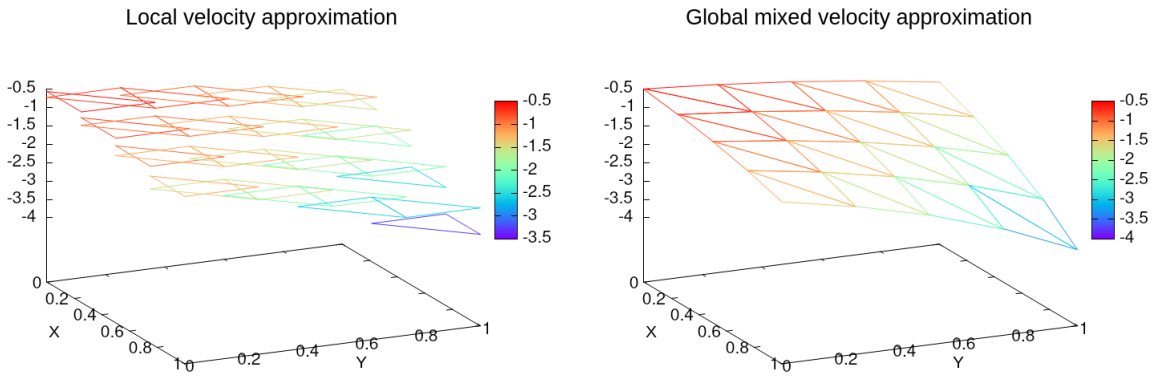

Figure 3. Approximations for the first component of the Darcy velocity with $n = 4$. On the left the local strategy (13a) is used, while the global mixed approach (15) is employed on the right.

5 Conclusions

As shown in Fig. 1, the mixed post-processing strategy (15) was able to produce higher-order approximations for the Darcy velocity than the standard local method (13a). The convergence rate was improved by one order in the L^2 norm, and by two if we consider the norm of the divergence as well. Furthermore, the velocity fields provided by (15) are also $H(\mathrm{div})$-conforming, leading to better mass-conservation properties. The combination of those facts results in significantly more accurate velocities when using the mixed approach, as illustrated by Fig. 3. On the other hand, the post-processed pressure obtained from (15) has the same convergence rate as the original pressure approximation, despite having smaller absolute errors.

For the effective stress approximation, all the strategies considered here provided almost identical L^2 errors. The difference between such strategies only becomes apparent when analyzing the divergence approximation. While the local approach (13b) only reached linear convergence for the divergence, strategy (17) with $\mathfrak{g}^m_h = -\boldsymbol{\mathcal{K}}\,\boldsymbol{z}^m_{h,G}$ converged quadratically. The divergence results for (17) with $\mathfrak{g}^m_h = \nabla p^m_h$ are still better than those obtained by (13b), but fail to reach optimal convergence rates in the $H(\mathrm{div})$ norm. As a final note, we remark that the stress fields provided by (17) are $H(\mathrm{div})$-conforming, and therefore one can expect better balanced inter-element tractions.

Acknowledgements. The authors thankfully acknowledge the financial support from the research agencies. This work was funded by the National Council for Scientific and Technological Development - CNPq under grants

304192/2019-8 and 140400/2021-4 and by the São Paulo Research Foundation (FAPESP) under grant 2013/07375-0.

Authorship statement. The authors hereby confirm that they are the sole liable persons responsible for the authorship of this work, and that all material that has been herein included as part of the present paper is either the property (and authorship) of the authors, or has the permission of the owners to be included here.

References

[1] V. Terzaghi. Die berechnug der durchlassigkeit des tones aus dem verlauf der hydromechanischen spannungserscheinungen. *Sitzungsber. Akad. Wiss.(Wien). Math.-Naturwiss. Kl., Abt. Iia*, vol. 132, pp. 125–138, 1923.
[2] M. A. Biot. General theory of three-dimensional consolidation. *Journal of Applied Physics*, vol. 12, n. 2, pp. 155–164, 1941.
[3] D. A. Walters, A. Settari, and P. R. Kry. Poroelastic effects of cyclic steam stimulation in the cold lake reservoir. volume All Days of *SPE Western Regional Meeting*, pp. SPE–62590–MS, 2000.
[4] P. Teatini, M. Ferronato, G. Gambolati, and M. Gonella. Groundwater pumping and land subsidence in the emilia-romagna coastland, italy: Modeling the past occurrence and the future trend. *Water Resources Research*, vol. 42, n. 1, 2006.
[5] T. Roose, P. A. Netti, L. L. Munn, Y. Boucher, and R. K. Jain. Solid stress generated by spheroid growth estimated using a linear poroelasticity model. *Microvascular Research*, vol. 66, n. 3, pp. 204–212, 2003.
[6] C. C. Swan, R. S. Lakes, R. A. Brand, and K. J. Stewart. Micromechanically based poroelastic modeling of fluid flow in Haversian bone. *Journal of Biomechanical Engineering*, vol. 125, n. 1, pp. 25–37, 2003.
[7] M. A. Murad and A. F. Loula. Improved accuracy in finite element analysis of Biot's consolidation problem. *Computer Methods in Applied Mechanics and Engineering*, vol. 95, n. 3, pp. 359–382, 1992.
[8] M. A. Murad and A. F. D. Loula. On stability and convergence of finite element approximations of Biot's consolidation problem. *International Journal for Numerical Methods in Engineering*, vol. 37, n. 4, pp. 645–667, 1994.
[9] M. A. Murad, V. Thomée, and A. F. D. Loula. Asymptotic behavior of semidiscrete finite-element approximations of biot's consolidation problem. *SIAM Journal on Numerical Analysis*, vol. 33, n. 3, pp. 1065–1083, 1996.
[10] C. Taylor and P. Hood. A numerical solution of the Navier-Stokes equations using the finite element technique. *Computers & Fluids*, vol. 1, n. 1, pp. 73–100, 1973.
[11] D. Boffi, F. Brezzi, and M. Fortin. *Mixed Finite Element Methods and Applications*, volume 44 of *Springer Series in Computational Mathematics*. Springer, 2013.
[12] G. Aguilar, F. Gaspar, F. Lisbona, and C. Rodrigo. Numerical stabilization of Biot's consolidation model by a perturbation on the flow equation. *International Journal for Numerical Methods in Engineering*, vol. 75, n. 11, pp. 1282–1300, 2008.
[13] A. F. Loula, F. A. Rochinha, and M. A. Murad. Higher-order gradient post-processings for second-order elliptic problems. *Computer Methods in Applied Mechanics and Engineering*, vol. 128, n. 3, pp. 361–381, 1995.
[14] P. A. Raviart and J. M. Thomas. A mixed finite element method for second order elliptic problems. In W. Wunderlich, E. Stein, and K. J. Bathe, eds, *Math. Aspects of the F.E.M.*, number 606 in 1, pp. 292–315. Springer-Verlag, 1977.
[15] G. Taraschi, A. S. Pinto, C. O. Faria, and M. R. Correa. On the application of a global post-processing strategy for stress recovery in nearly-incompressible elasticity problems. *Proceedings of the Ibero-Latin-American Congress on Computational Methods in Engineering*, vol. 1, 2022.